Journal of Applied Electrochemistry (2005) 35:1145–1156
DOI 10.1007/s10800-005-9022-x

Electrochemical characterization of $La_{0.8}Sr_{0.2}MnO_3$-coated NiO as cathodes for molten carbonate fuel cells

BO HUANG[1,2,*], SHAO-RONG WANG[2], QING-CHUN YU[3], YU LIU[1] and KE-AO HU[1,3]
[1]*State Key Laboratory of Metal Matrix Composites, Shanghai Jiaotong University, Shanghai, 200030, P.R. China*
[2]*Shanghai Institute of Ceramics, Chinese Academy of Sciences (SICCAS), 1295 Dingxi Road, Shanghai, 200050, P.R. China*
[3]*Institute of Fuel Cell, Shanghai Jiaotong University, Shanghai, 200030, P.R. China*
*(*author for correspondence, fax: +86-21-62822012; e-mail: huangbo2k@hotmail.com)*

Received 29 September 2004; accepted in revised form 27 June 2005

Key words: cathode, coating, EIS, molten carbonate fuel cell, nickel oxide

Abstract

$La_{0.8}Sr_{0.2}MnO_3$ was coated on porous NiO cathode using a simple combustion process. X-ray diffraction (XRD) and scanning electron microscopy (SEM) were employed in the cathode characterizations. The electrochemical behavior of $La_{0.8}Sr_{0.2}MnO_3$-coated NiO cathodes (LSM–NiO) were also evaluated in a molten 62 mol%Li_2CO_3 + 38 - mol%K_2CO_3 eutectic at 650 °C under the standard cathode gas condition by electrochemical impedance spectroscopy (EIS). The impedance response of the NiO and LSM–NiO cathode at different immersion times is characterized by the presence of depressed semicircles in the high frequency range and an extension at low frequencies. Impedance analysis showed that the behavior of the developed cathode was similar to that of the conventional nickel oxide cathode. The LSM–NiO showed a lower dissolution and a better catalytic efficiency superior to the state-of-the-art NiO value. Thus the cathode prepared with coating method to coat $La_{0.8}Sr_{0.2}MnO_3$ on the surface of NiO cathode is able to reduce the solubility of NiO to lengthen the lifetime of MCFC while maintaining the advantages of NiO cathode. The LSM–NiO shows promise as an alternate cathode in molten carbonate fuel cells (MCFCs).

1. Introduction

The molten carbonate fuel cell (MCFC) is one of the most promising energy conversion devices that convert chemical energy in fossil fuels into electricity. It can be applied not only to alternative thermal power plants but also dispersed power plants and integrated coal gasification combined cycle power plants (IGCC). However, the state-of-the-art NiO cathode has a relatively high solubility in the electrolyte which can be Li_2CO_3–/K_2CO_3, Li_2CO_3–/Na_2CO_3 or related alkali molten carbonate eutectics. This dissolution leads to the formation of Ni^{2+} and eventually causes short-circuiting of the cell [1, 2]. In order to improve the chemical stability of the cathode against molten carbonate, many studies have been carried out [3–7]. More basic molten carbonate melts such as Li/Na carbonate eutectic have been used to decrease the Ni dissolution rate in the melt. Alkaline earth metal oxides or carbonates based on Ba or Sr have also been used as additives for the electrolyte to enhance the chemical stability of the NiO cathode by decreasing the acidity of the electrolyte, however, cell performance is largely degraded as a trade-off [8–10]. In addition, several ceramic materials like $LiFeO_2$, $LiCoO_2$, Li_2MnO_3 and $LiCo_{1-x}Ni_xO_2$ were also investigated as replacement materials for the NiO cathodes because of their extremely low solubility in the carbonate melts [11]. However, these materials are of lower electrical conductivity than NiO. In addition, these cathodes of large size are not easily fabricated due to the brittleness of the materials. Meanwhile, several research studies have shown that modification of the NiO cathode by coating it with $LiCoO_2$, $LiFeO_2$, $La_{0.8}Sr_{0.2}CoO_3$, CeO_2 or Nb_2O_5 [3, 12–22], or mixing an oxide of alkali earth or transition metal [23–25], effectively suppresses NiO dissolution in molten carbonate with negligible performance degradation. Among those choices, the coating method is being watched with keen interest because the small amount of stabilizer deposited on the internal surface of NiO prevents NiO dissolution without the loss of electrical conductivity of the cathode. The solubility in molten carbonate of the stabilizer-coated NiO cathode decreased to 46–93% of that for an uncoated cathode dependent on the experimental conditions [3, 16–18].

In this study, a novel NiO cathode was prepared by coating $La_{0.8}Sr_{0.2}MnO_3$ grains on a porous NiO cathode using an auto-ignited combustion process with a citrate–metal nitrate precursor. The present work aimed to study the electrochemical behavior of the new cathode material in molten carbonates. The study was conducted using electrochemical impedance spectroscopy (EIS). The phases and microstructures of the cathode materials before and after immersion in molten carbonate were analyzed by X-ray diffraction (XRD) and scanning electron microscopy (SEM), respectively. The dissolution of the new cathode material in molten carbonates was evaluated using melt analysis.

2. Experimental

2.1. *Starting materials*

The material system used was based on carbonyl nickel powder, solvent, dispersant, binder and plasticizer. The carbonyl nickel particles (purity: 98%; Shanghai Jinjiang Metal Powder Ltd., China) have a perfect orbicular shape and a narrow size distribution of 2.2–2.8 μm. The solvent system used consisted of an azeotropic mixture of cyclohexanone and butyl alcohol in order to avoid differential evaporation. Glycerol trioleate was used as dispersant. Polyvinylbutyl (PVB) and polyethylene glycol (PEG 200) were used as binder and plasticizer, respectively. The PVB binder was supplied as a free flowing fine-grained powder and the PEG plasticizer was obtained in liquid form. All the organic additives were supplied by Shanghai Chem. Ltd., China.

2.2. *Preparation of porous NiO cathodes*

Porous nickel cathodes were prepared by a tape casting and subsequent sintering process. The slurries for the tape casting process were fabricated by a ball milling method that included two steps. In the first step, 50 g of nickel powder were added to 1 g dispersant. The ingredients were mixed thoroughly with 40 g cyclohexanone/butyl alcohol solvents, and the slurry was ball milled for 4 h in order to break weak agglomerates. Secondly, 5 g PVB and 5 g PEG were added to the above system and the resulting slurry was ball milled for an additional 4 h. After the mixing and the homogenization of the slurry were completed, the slurry was degassed using a vacuum pump (pressure: 200 mbar absolute) and cast on a casting surface of polyethylene film by a ''doctor-blade'' method. The cast tapes were allowed to dry at room temperature for 48 h. After the solvent in the tapes was completely evaporated, the nickel green tapes were obtained. The sintering process of the green tapes was carried out in 75 vol.%H_2/25 vol.%N_2 atmosphere at 850 °C for 0.5 h. The nickel plates were then oxidized in the air at 850 °C for 6 h, the porous NiO cathodes were thus obtained. Detailed procedures for cathode preparation and sintering are presented elsewhere [26, 27].

2.3. *$La_{0.8}Sr_{0.2}MnO_3$ coating*

$La_{0.8}Sr_{0.2}MnO_3$ precursor gel was prepared as follows. Initially, stoichiometric amounts of lanthanum nitrate ($La(NO_3)_3{\cdot}6H_2O$), strontium nitrate ($Sr(NO_3)_2$) and manganese nitrate ($Mn(NO_3)_2$) were dissolved in distilled water with constant stirring. Then, a stoichiometric amount of citric acid ($C_6H_8O_7{\cdot}H_2O$), which is a chelating agent and fuel, was also dissolved in this solution. The stoichiometric ratio of citric acid to nitrates was calculated according to Jain et al. [28]. The La^{3+} concentration in the transparent solution was 0.16 mol dm^{-3}. The solution pH was maintained between 7 and 8.The sintered porous NiO sheets were dipped in the above solution and evacuated using a vacuum pump set to an absolute pressure of 200 mbar for 30 min so that the solution filled the pores of the NiO sheets. Then the NiO sheets were kept at 450 °C for several minutes and heat-treated at 850 °C for 6 h. This procedure was repeated several times to have a uniform coating. The flow chart for the coating is given in Figure 1.

2.4. *Electrochemical characterization*

The electrochemical characterization of the new cathode materials was performed on the porous electrode/molten carbonates interface by means of EIS. The eutectic mixture of alkali carbonate, 62 mol%Li_2CO_3–38 mol%K_2CO_3, was made up from AR grade anhydrous reagents (Shanghai chem. Ltd., China) that had been dried in a furnace at 150 °C. The mixture was purified by a sequence of the following treatments:

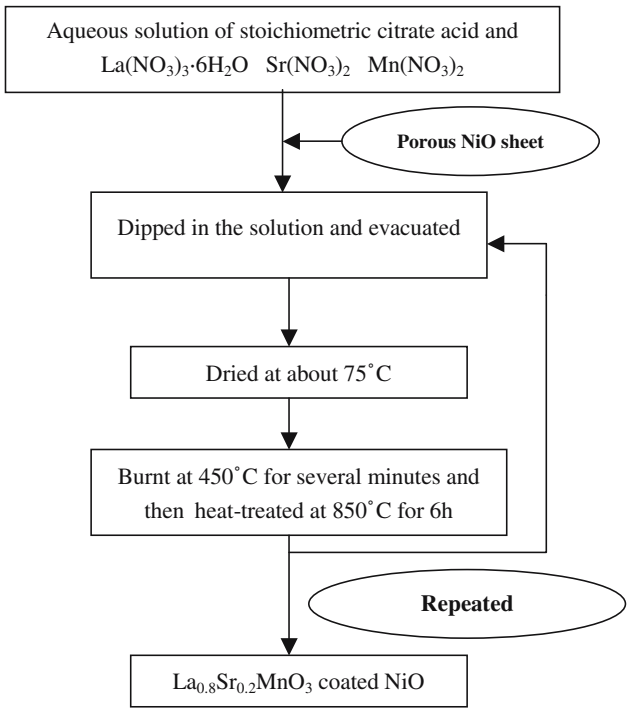

Fig. 1. Flow chart for the preparation process of $La_{0.8}Sr_{0.2}MnO_3$-coated NiO cathode.

vacuum drying at 350°C,fusion/pumping treatment at 700°C and bubbling of pure CO_2. Gases were of high purity grade and were additionally treated with molecular sieves 5A and anhydrous $Mg(ClO_4)_2$ to remove traces of water [29, 30].

Experimental techniques, apparatus and the electrochemical cell assembly have been described previously [27]. The electrodes (Z 2.4 cm × 0.08 mm) cut out from sintered NiO and $La_{0.8}Sr_{0.2}MnO_3$-coated NiO (LSM-NiO) plates in the air were inserted in the carbonate melt and the cell temperature was kept at 650 °C. The EIS measurements were started 2 h after immersion in the melt in order to obtain a sufficiently stabilized system necessary for an AC-impedance experiment. Various measurements were made from 0 to 200 h under a 0.67 atm CO_2–0.33 atm O_2 gas mixture. The AC impedance measurements were recorded by means of Solaritron Electrochemical Interface 1260 and Solaritron Frequency Response Analyzer controlled by ZPLOT. All equivalent circuit fittings for impedance results were done by ZVIEW. A 5-mV perturbation amplitude was applied with a frequency scanning range of 10–100 kHz at five points per frequency decade.

2.5. *Structural characterization and chemical analysis*

The structure of the cathode samples sintered at 850 °C in the air for 6 h before and after the electrochemical tests was characterized by scanning electron microscopy (SEM, PHLIPS 515). Transmission electron microscopy (TEM, JEM 2010) and X-ray diffraction (XRD, D/max-3A, Cu$K\alpha$) were performed to observe the morphology and analyze the phase of the combustion-synthesized powder, respectively. The porosity and densities of various cathodes were measured by Archimedes' principle in distilled water. In order to determine the structure of the samples after immersion in the molten carbonate, they should be first dissolved in 50 vol.% acetic acid/50 vol.% anhydride mixture aimed to removing the carbonates at the samples surface. Solubility was determined by removing a 0.5 g of molten carbonate from the melts at the appointed time using an alumina rod. Solubility measurements were repeated until their value became concentration that was regarded as the equilibrium solubility. Inductively coupled plasma spectroscopy was carried out to analyze the metal ions equilibrium solubility in the molten carbonate after 200 h of continuous exposure to the molten carbonate.

3. Results and discussion

3.1. *Microstructural characterization*

3.1.1. *Cathode characterization*

Plot of pore diameter vs. cumulative volume of various cathodes is given in Figure 2. The average pore diameter of the pure nickel cathode was about 12 μm. After being coated with $La_{0.8}Sr_{0.2}MnO_3$ and calcined in the air at

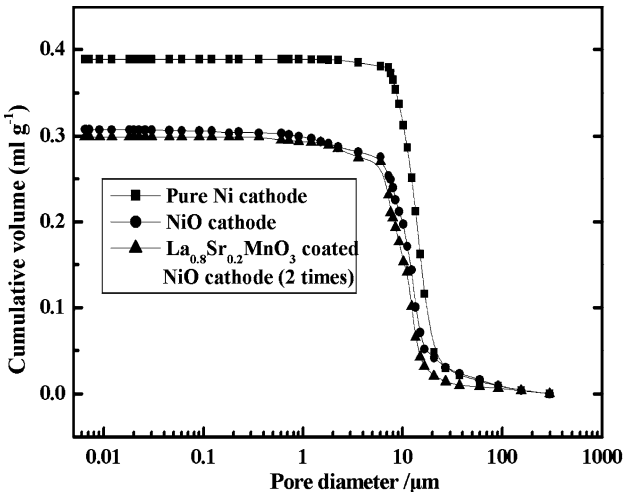

Fig. 2. Plot of pore diameter vs. cumulative volume of various cathodes.

850 °C for 6 h, the nickel was oxidized and the average pore diameter decreased to about 9 μm. Table 1 shows textural characterization of the Ni cathode, NiO cathode and LSM–NiO cathode. It could be seen that the nickel cathode had the largest porosity and lowest density. After being oxidized in the air at 850 °C for 6 h, its porosity decreased from 81.08 to 75.96% and the density increased from 2.09 to 2.19 g cm^{-3} due to the sintering effect. In comparison with the NiO cathode, the LSM–NiO cathode had a lower porosity (62.18%) and a larger density (2.33 g cm^{-3}), which was due not only to the sintering effect but also to the coating of $La_{0.8}Sr_{0.2}MnO_3$ on the porous surface of this cathode. The decrease in porosity and pore size does not mean that the performance of the cell will be poor after a long-term operation. In fact, large porosity and pore size are not always beneficial to high performance of the MCFC. It is well known that a cathode with high performance should be of appropriate porosity (60∼80 vol.%)and pore size distribution (6∼10 μm), so that the best balance between the solid, liquid and gas phases is maintained during the MCFC operation. Evidently, the LSM–NiO cathode prepared was sufficient to satisfy the requirement of the MCFC operation.

3.1.2. *SEM characterization*

Figure 3 shows the cross-section SEM micrographs of Ni, NiO and LSM–NiO cathodes, respectively. The morphological difference between NiO and LSM–NiO cathode could be attributed to the $La_{0.8}Sr_{0.2}MnO_3$ coating on nickel oxide particles surfaces followed by sintering, the particles of LSM–NiO cathode tended to agglomerate together. The $La_{0.8}Sr_{0.2}MnO_3$- coated NiO

Table 1. Porosity and bulk density of various cathodes

Porous cathode	Ni cathode	NiO cathode	LSM–NiO cathode
Porosity/%	81.08	75.96	62.18
Density/g cm^{-3}	2.09	2.19	2.33

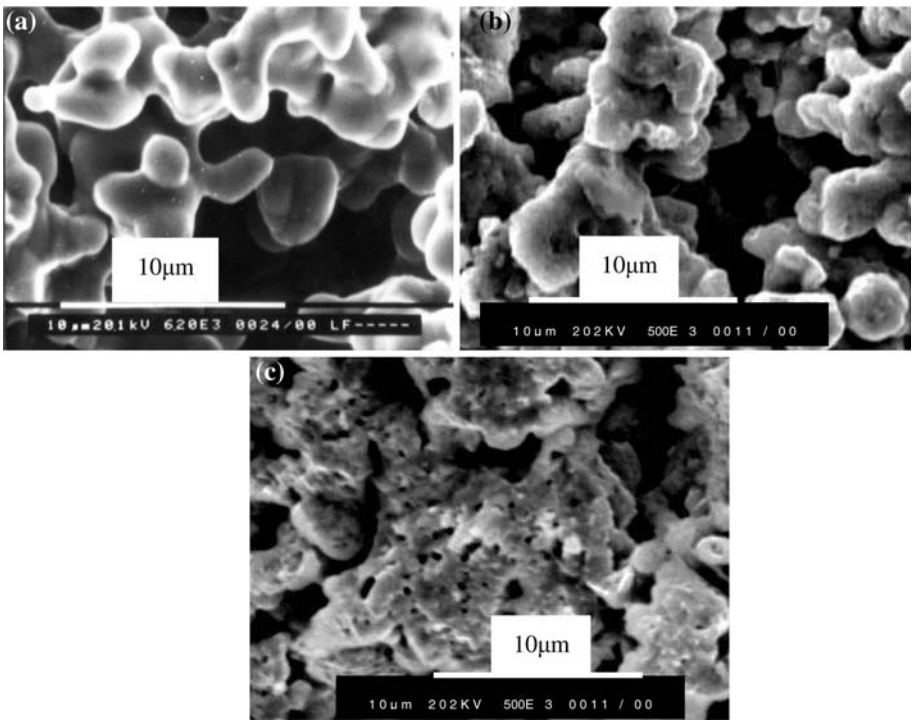

Fig. 3. SEM cross-section micrographs of (a) Ni cathode; (b) NiO cathode; (c) LSM–NiO cathode.

cathode had a good pore structure. However, detailed pore volume distribution analysis needs to be carried out to determine the actual porosity and pore size distribution. In comparison with nickel and nickel oxide particles, the surfaces of the pre-treated NiO particles were covered with many tiny grains, which were sintered with the NiO particles. Some small holes were also observed on the $La_{0.8}Sr_{0.2}MnO_3$ coating due to the release of gases, such as H_2O, CO_2 and N_2, during the combustion procedure of the citrate–nitrate solution in the pores.

Figure 4 shows scanning electron micrographs of pure NiO and LSM–NiO cathodes before and after exposure to molten carbonate for 200 h under the standard cathode gas condition (CO_2:O_2, 67:33%). After electrochemical testing, the pure NiO cathode surface showed marked morphological changes due to the dissolution. By comparison, no significant differences in the particle size and the surface morphology of $La_{0.8}Sr_{0.2}MnO_3$-coated NiO cathode were observed before and after immersion for 200 h.

3.1.3. *XRD characterization*

Figure 5 shows the X-ray diffraction patterns of $La_{0.8}Sr_{0.2}MnO_3$ powders obtained from the gel after heat treatment at different temperatures ranging between 450 and 850 °C. The X-ray diffraction pattern for the gel presents no diffraction peaks, which indicates an amorphous phase. It is clearly seen that the compound formation starts only at 650 °C and crystalline product could be obtained at 850 °C. From the TEM image of the synthesized powder as shown in Figure 6, $La_{0.8}Sr_{0.2}MnO_3$ grains with nm size could be clearly observed. The $La_{0.8}Sr_{0.2}MnO_3$ formation onto the nickel oxide cathodes was confirmed by matching the individual peaks. Figure 7 shows the XRD pattern of $La_{0.8}Sr_{0.2}MnO_3$ coated-NiO sintered at 850 °C. Individual peaks correspond to $La_{0.8}Sr_{0.2}MnO_3$ and NiO are marked in the figure. From the above analysis, it can be inferred that the ultra fine $La_{0.8}Sr_{0.2}MnO_3$ grains may coat the surface of the porous nickel oxide sheet by burning the citrate + nitrate solution that filled the pores and covered the surface of the porous nickel oxide sheets.

3.2. *Solubility test*

The dissolution curves of NiO and LSM–NiO cathodes in molten 62 mol%Li_2CO_3 + 38 mol%K_2CO_3 eutectic are given in Figure 8. The experimental conditions were kept at 650 °C under a 0.67 atm CO_2/0.33 atm O_2 atmosphere. The dissolution of NiO and LSM–NiO increased significantly with time before 100 h and saturated after about 100 h. The NiO cathode had a solubility of 34.3 mol ppm (Ni^{2+}) in the $(Li_{0.62}K_{0.38})_2CO_3$ melts after 200 h, which is similar to the results reported by N. Motohira et al. [31]. In contrast, the solubility of the LSM–NiO cathode was only 12.0 mol ppm (Ni^{2+}).

The results of solubility tests show that the coating of $La_{0.8}Sr_{0.2}MnO_3$ on the surface of NiO can significantly retard the dissolution of NiO in molten carbonates. It should be noted that the coating on the surface of the NiO particles consisted mainly of ultrafine $La_{0.8}Sr_{0.2}MnO_3$ grains, but not a complete $La_{0.8}Sr_{0.2}MnO_3$ film. Although the $La_{0.8}Sr_{0.2}MnO_3$ grains were

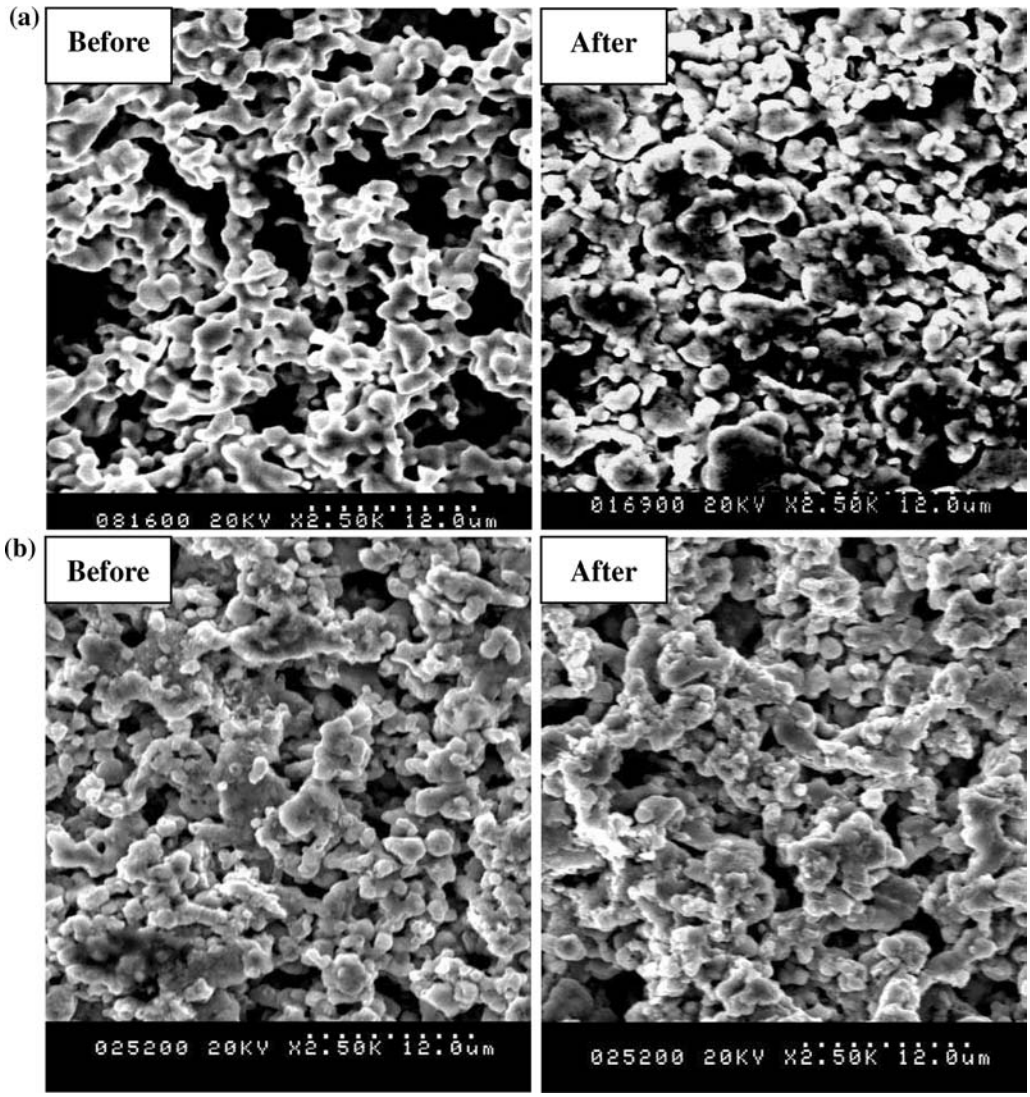

Fig. 4. SEM micrographs corresponding to the two cathode samples before and after testing: (a) Pure NiO cathode; (b) LSM–NiO cathode.

tightly sintered with the NiO particles due to the high instantaneous temperature during the combustion procedure [28], the released gases such as H_2O, N_2 and CO_2 gave rise to holes in the coating, as is shown in Figure 3(c), which means that the coating only reduces the contacting area of the NiO particles with the melts,

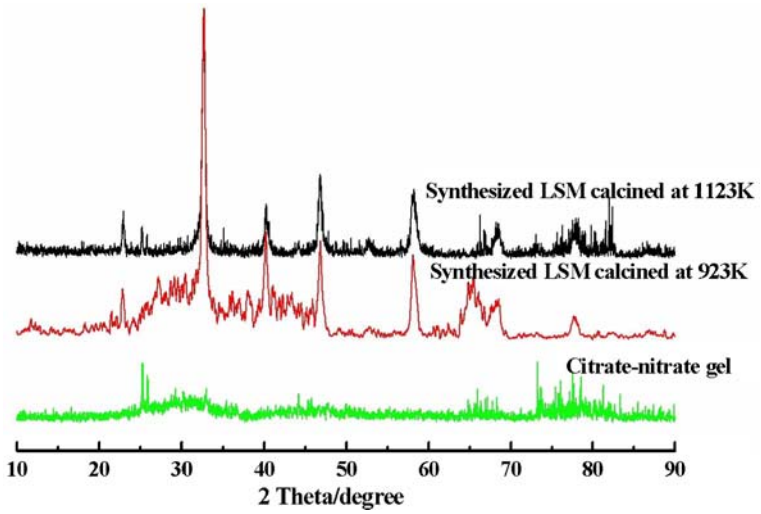

Fig. 5. X-ray diffraction patterns of $La_{0.8}Sr_{0.2}MnO_3$ obtained after different heat treatment of the gel precursor.

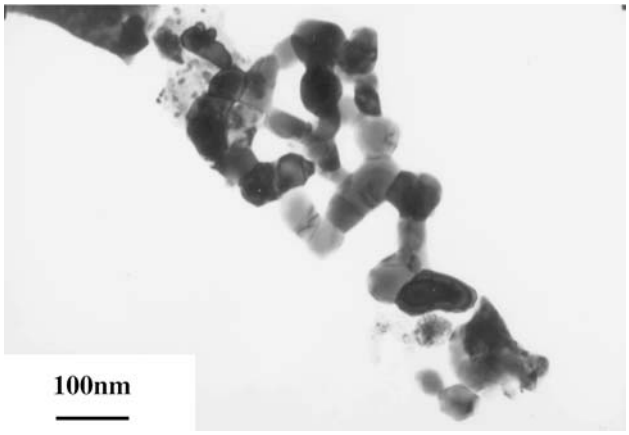

Fig. 6. TEM image of combustion-synthesized $La_{0.8}Sr_{0.2}MnO_3$ powder calcined at 850 °C for 6 h.

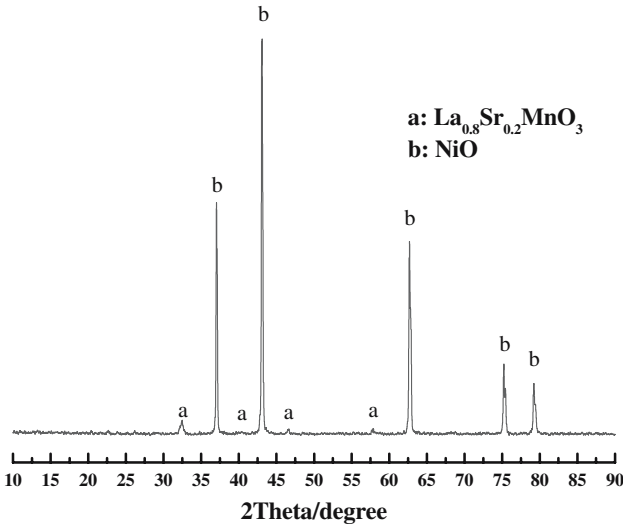

Fig. 7. X-ray diffraction patterns of $La_{0.8}Sr_{0.2}MnO_3$-coated porous NiO cathode sintered at 850 °C.

but does not completely separate the NiO particles from the melts.

The aim of coating the NiO cathode with $La_{0.8}Sr_{0.2}MnO_3$ is to prolong the time to short circuit of the MCFC. Since geometric protection cannot decrease the equilibrium solubility but the rate of dissolution. However, a coating with tiny holes cannot completely prevent the dissolution of the inner NiO and the content of nickel ions in the melts will eventually reach the value of that for pure NiO, but the time for this to occur is dramatically extended. This indicates that the dissolution rate (mol ppm h^{-1}) of LSM–NiO is lower than that of pure NiO. So we infer that the MCFC using LSM–NiO as the cathode has a longer life than that using conventional NiO as the cathode. Further research studies will be required to compare the efficiency of a cell using a NiO cathode with that using a $La_{0.8}Sr_{0.2}MnO_3$-coated NiO cathode.

3.3. *Electrochemical impedance spectroscopy (EIS) study*

Figure 9 depicts the electrochemical impedance spectra for the two cathode materials in a eutectic 62 mol% Li_2CO_3 + 38 mol% K_2CO_3 at 650 °C under a 0.67 atm CO_2/0.33 atm O_2 gas mixture at different immersion time. As can be seen from the corresponding Nyquist plots, the impedance response of the two cathode materials at different immersion times is characterized by the presence of depressed semicircles in the high frequency range and an extension at low frequencies. The high frequency plot has been associated with the charge transfer process while the low frequency loop to a slow process (mass transfer or slow homogeneous reactions). At high frequencies, the plot converged to a

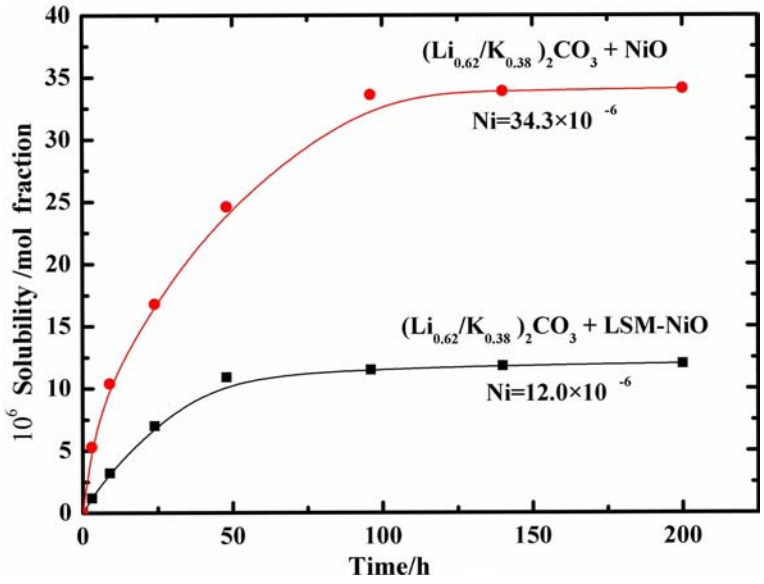

Fig. 8. Equilibrium solubility of nickel ions in the $(Li_{0.62}K_{0.38})_2CO_3$ melts shown as a function of immersion time ($T = 650$ °C, $p(CO_2) = 0.67$ atm, $p(O_2) = 0.33$ atm).

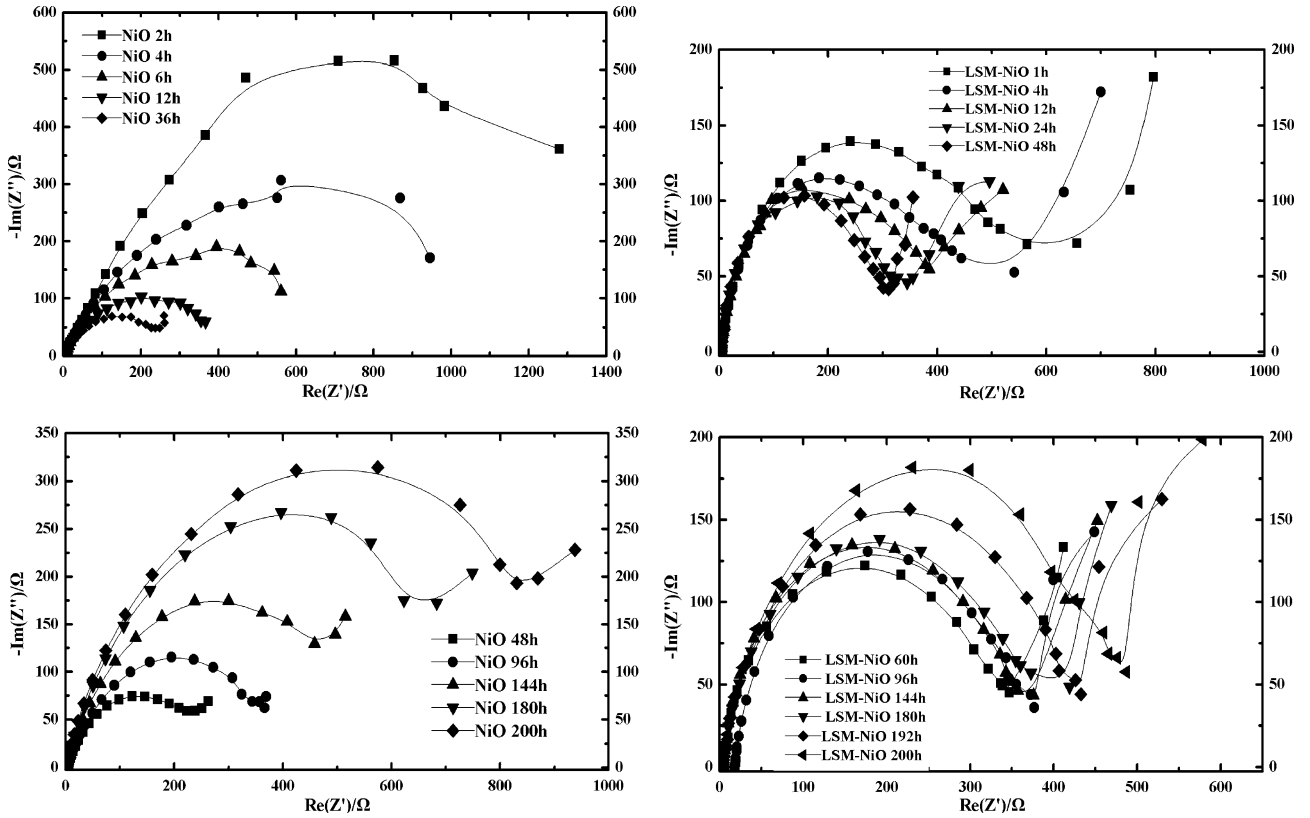

Fig. 9. Nyquist impedance spectra obtained for two samples in the frequency range of 10 mHz–100 kHz as a function of immersion time at 650 °C in standard cathode gas atmosphere (CO_2:O_2, 67:33%).

value on the abscissa (real axis) as shown in Figure 9, giving the electrolytic resistance, R_Ω.

For the oxygen reduction reaction on the two cathode materials in Li/K eutectic melts at different immersion time, the empirical plots of impedance on the complex plane were semicircles. The center of the semicircle lies on the real axis, provided that the double layer functions as a perfect capacitor. However, in many cases, the center of the semicircle does not lie on the real axis. They may be looked upon as semicircles rotated in the clockwise sense around the origin by a certain angle θ, as seen in Figure 10. This phenomenon may be called a dispersion effect. In the study of the oxygen-evolution reaction, Iseki et al. [32] proposed that the dispersion effect could be simulated by a resistor in inverse proportion to the frequency ω. Wang et al. [33] proved that the dispersion effect could be represented by $\omega \times C \times \mathrm{ctg}\,(\beta \times \pi/2)$, where β represents the dispersion coefficient and $\beta = 1 - \theta(2/\pi)(0 < \beta \leq 1)$. The smaller β is, the more obvious the dispersion effect is. The dispersion effect may be attributed to the non-uniform electric field at the electrode/electrolyte interface owing to the roughness of electrode surface, or the variety of relaxation times with adsorbed species on the electrode surface [34–36]. In the present case, it may result from porosity in the cathode materials. Unfortunately, at present, a quantitative association of dispersion with porosity cannot be obtained. The equivalent circuit for the electrochemical impedance spectra may be described

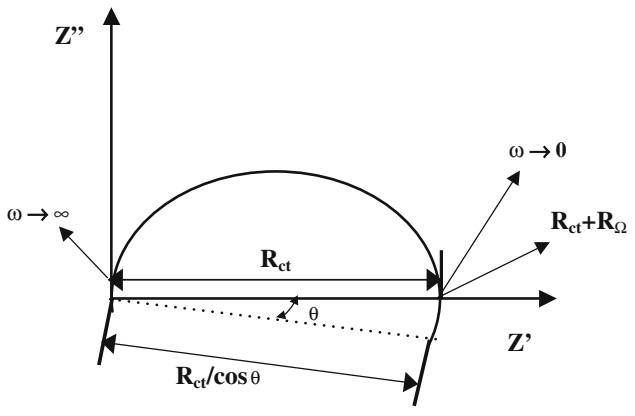

Fig. 10. Sketch map of rotation of semicircle on the complex plane.

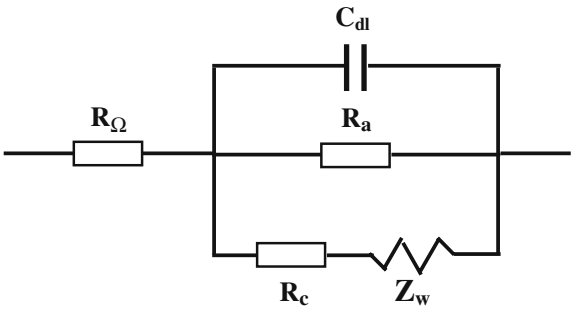

Fig. 11. Equivalent circuit corresponding to rotation of semicircle on the complex plane.

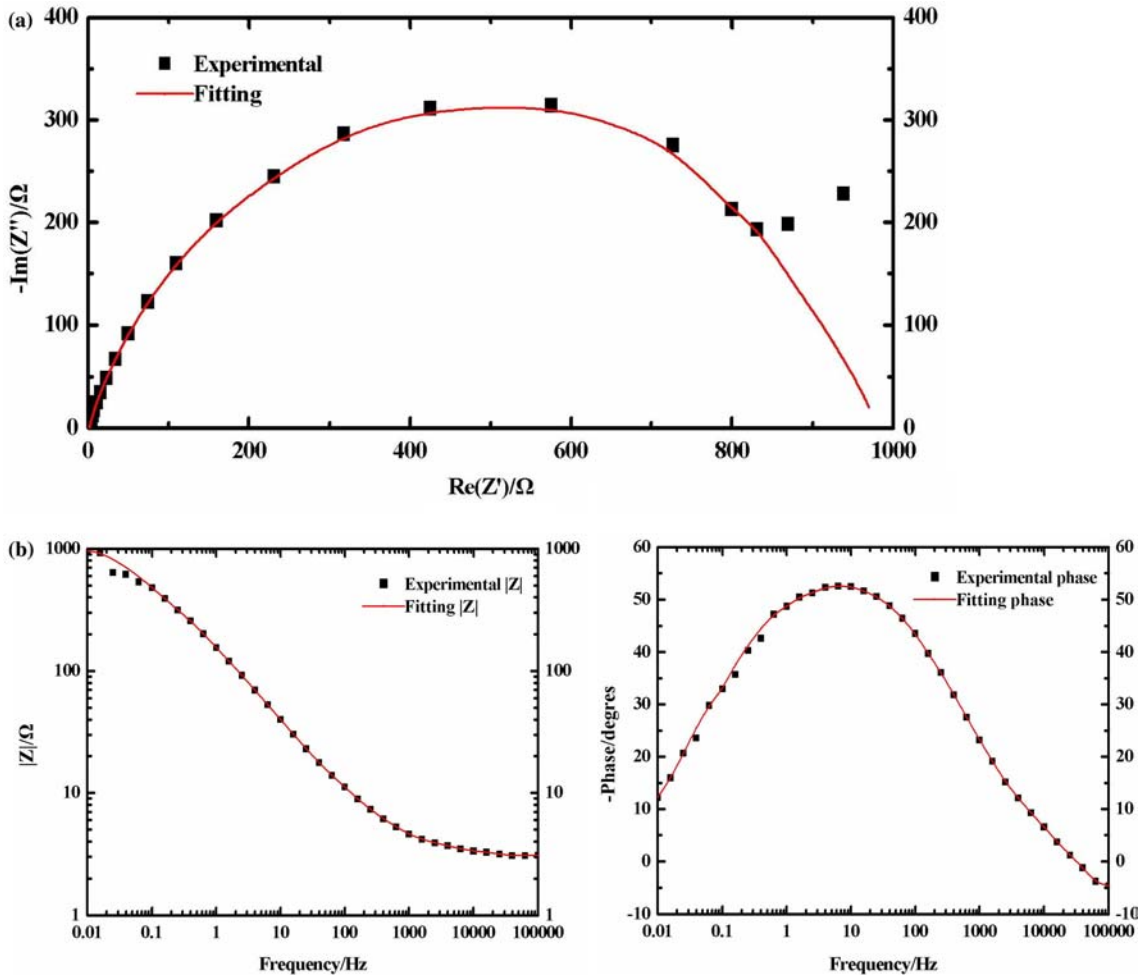

Fig. 12. Measured impedance spectra for NiO cathode in the frequency range of 10 mHz to 100 kHz at 200 h at 650 °C in standard cathode gas atmosphere (CO_2:O_2, 67:33%) compared to spectra calculated following Equation (3): (a) Nyquist plot; (b) Bode plot.

by the equivalent circuit of Figure 11, where R_Ω represents the molten-salt resistance, C_{dl} the double-layer capacitance, R_a the anodic charge transfer resistance, R_c the cathodic charge transfer resistance, and Z_w the diffusion-induced Warburg resistance. Thus, taking into account the dispersion effect, the electrochemical impedance for the circuit in Figure 11 may be expressed by Equation (1)

$$Z = R_\Omega + 1/[j\omega C_{dl} + \omega C_{dl}\,\mathrm{ctg}(\beta(\pi/2)) + 1/R_a + 1/(R_c + Z_w)] \quad (1)$$

where $\omega\ C_{dl}\ \mathrm{ctg}(\beta(\pi/2))$ represents the resistance caused by the dispersion effect. The Warburg resistance may be expressed by Equation (2) [37]

$$Z_w = A_w(j\omega)N_w \quad (2)$$

where A_w represents the modulus of Warburg resistance, and N_w is the Warburg coefficient, $-0.5 \le N_w < 0$.

It is well known that R_c is much greater than Z_w at high frequency. Thus Equation (1) may be simplified to

$$Z = R_\Omega + 1/[j\omega C_{dl} + \omega C_{dl}\,\mathrm{ctg}(\beta\pi/2)) + 1/R_{ct}] \quad (3)$$

where $R_{ct} = R_a \cdot R_c/(R_a + R_c)$ represents the charge transfer resistance.

All impedance spectra were fitted to Equation (3) which corresponded to the equivalent circuit that considered both the non-uniformity of electric field at the electrode/electrolyte interface owing to the roughness of electrode surface and the variety of relaxation times with adsorbed species on the electrode surface. In all cases, the fits were very satisfactory in the whole frequency range. The NiO and LSM–NiO cathode samples can be seen in Figures 12 and 13, where the experimental and fitted data are depicted in the Nyquist and Bode diagrams for two cathode samples at 200-h immersion. All experimental plots could be well described theoretically with the equivalent circuit model. The values of these parameters are given in Tables 2 and 3.

As can be seen from Figure 9 and Tables 2 and 3, the molten-salt resistance R_Ω is almost independent of immersion time, which indicates that the Li/K eutectic melt is strong electrolyte. The diameter of the semicircular arc (denotes the charge transfer resistance R_{ct}) decreases sharply with time initially. This implies that, in the case of two cathode materials, the electrochem-

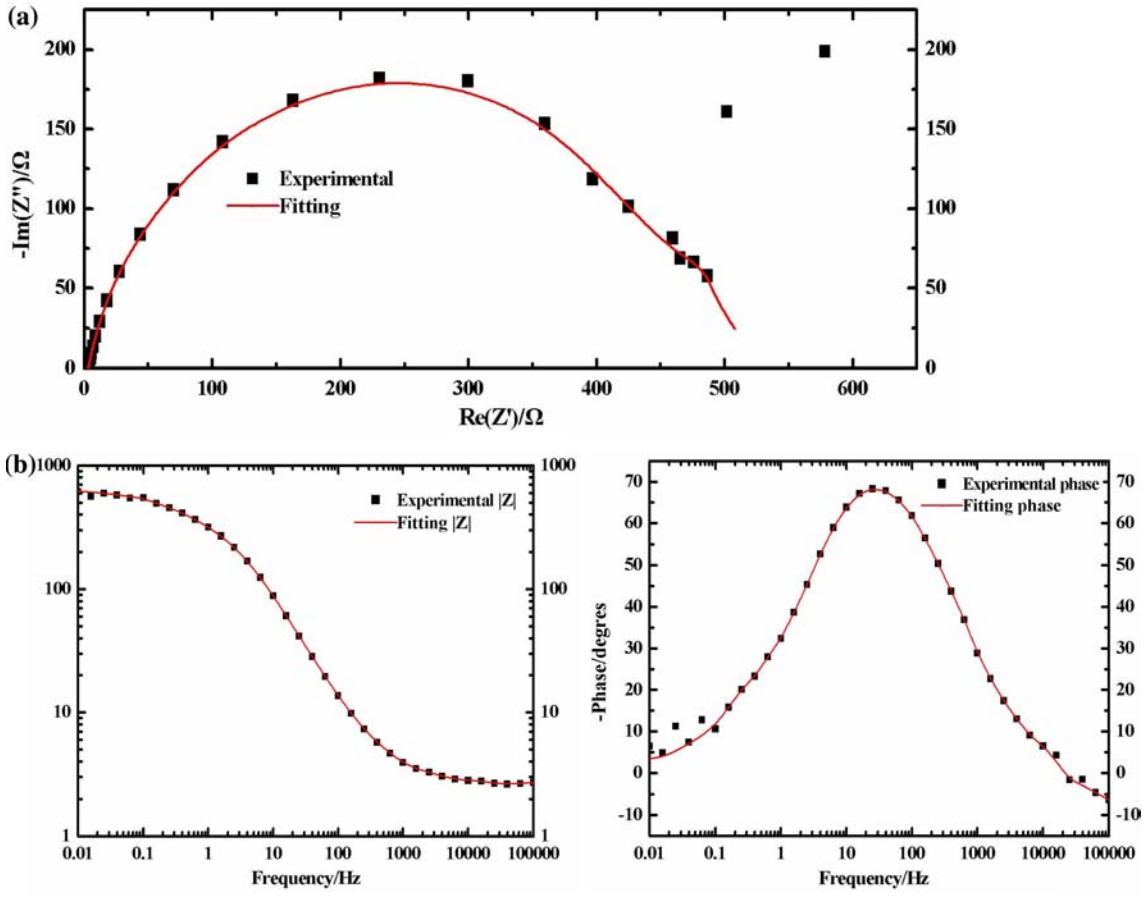

Fig. 13. Measured impedance spectra for LSM–NiO cathode in the frequency range of 10 mHz to 100 kHz at 200 h at 650 °C in standard cathode gas atmosphere (CO_2:O_2, 67:33%) compared to spectra calculated following Equation (3): (a) Nyquist plot; (b) Bode plot.

ical reaction rates are increasing rapidly with time. The reason may be the incorporation of lithium to its structure, which enhances its electronic conductivity. Then, the semicircular arc increases slightly with time suggesting that the corresponding electrochemical reaction rates are decreasing slowly with time (in terms of NiO, LSM–NiO, after 36 h, 48 h, respectively). The reason may be the slow dissolution of two cathode

Table 2. Fitting results for oxygen reduction on NiO electrode in Li/K eutectic melts at different immersion time (Atmosphere: 0.67 atm CO_2/0.33 atm O_2; T = 650 °C)

time/h	R_Ω/Ω	R_{ct}/Ω	R_{dl}/μF	θ/°	β
1	2.1485	2675.900	/	/	/
4	2.2398	999.260	2831.400	33.894	0.6234
6	2.3018	633.490	1777.400	33.453	0.6283
8	2.2036	531.850	1726.200	34.299	0.6189
10	2.3925	419.190	1241.800	35.009	0.6110
12	2.1745	382.380	1181.400	35.320	0.6076
20	2.3170	302.020	1033.700	36.107	0.5988
22	2.3222	288.920	1062.300	36.166	0.5982
24	2.2413	291.550	1077.900	36.230	0.5974
36	2.4384	271.150	996.130	36.290	0.5968
48	2.0634	296.630	895.840	36.816	0.5909
72	3.0407	338.280	1002.500	30.400	0.6622
96	3.0774	402.480	952.310	30.208	0.6644
120	2.6579	515.680	1071.800	26.172	0.7092
144	3.0106	546.720	1318.500	24.853	0.7239
168	2.0093	607.500	1285.000	24.982	0.7224
180	2.5596	803.880	1310.900	23.131	0.7430
192	2.0317	925.250	1199.500	22.758	0.7471
200	1.9347	948.830	1626.700	23.400	0.7400

Table 3. Fitting results for oxygen reduction on $La_{0.8}Sr_{0.2}MnO_3$ coated NiO electrode in Li/K eutectic melts at different immersion time (Atmosphere: 0.67 atm CO_2/0.33 atm O_2; $T = 650$ °C)

time/h	R_Ω/Ω	R_{ct}/Ω	$C_{dl}/\mu F$	$\theta/°$	β
0	1.4094	1054.10	210.13	34.138	0.6207
1	1.9704	535.65	122.36	34.220	0.6198
3	2.1148	468.81	139.30	36.209	0.5977
4	1.5464	404.19	189.07	37.523	0.5831
12	2.0176	350.19	307.51	37.111	0.5877
13	1.5905	328.72	156.21	36.825	0.5908
14	2.7162	316.81	163.16	36.659	0.5927
16	1.5463	313.03	165.16	36.715	0.5921
20	1.7250	302.79	174.06	37.158	0.5871
22	1.8454	314.78	190.27	38.273	0.5747
24	2.0970	317.00	194.08	37.315	0.5854
36	2.1906	341.43	216.07	38.635	0.5707
48	2.1881	295.44	241.84	39.223	0.5642
60	1.7926	345.52	281.54	39.560	0.5604
72	2.2073	355.13	319.06	37.264	0.5860
96	1.9949	373.76	303.79	36.583	0.5935
120	2.1760	363.18	333.65	35.486	0.6057
144	2.0389	379.76	303.79	35.560	0.6049
168	2.5063	389.67	312.19	34.209	0.6199
180	2.6748	431.42	299.60	33.369	0.6292
192	2.5748	436.70	328.46	31.025	0.6553
200	2.2454	498.26	348.46	32.635	0.6374

materials in molten carbonates. The variation of the charge transfer resistance with time for the NiO and LSM–NiO cathodes indicates that the dissolution process and charge transfer process are not taking place under constant conditions, rather the conditions at the cathode surface are modified with the time of exposure to the carbonates. These surface modifications affect dissolution process and electrochemical performance of cathode samples. Different authors have reported that NiO incorporates lithium cations from the molten carbonates during fuel cell operation. This lithium incorporation introduces modifications in the surface composition and, probably, affects the dissolution process and electrochemical performance. In the case of the two cathode samples, after an initial decrease, the charge transfer resistance increases gradually and eventually reaches a relatively constant value that depends on the immersion time. These two different steps indicate that the dissolution process and charge transfer process in these cathode samples are also affected by lithiation. Due to the introduction of Li^+ ions into the NiO lattice, Ni^{2+} ions are substituted by Ni^{3+} ions. In addition, we can also find that the semicircular arc of the LSM–NiO cathode is a little smaller than that of the pure NiO cathode at different immersion times in the high frequency region. This suggests that the $La_{0.8}Sr_{0.2}MnO_3$ coating has a slightly positive influence on the charge transfer processes associated with the oxygen reduction reaction. Therefore, we infer that $La_{0.8}Sr_{0.2}MnO_3$ favors the lithiation process, resulting in a mixed oxide with a higher Li^+ content that is a more conductive and stable cathode [38]. The differences between the electrochemical impedance spectra corresponding to the NiO and LSM–NiO cathodes (Figure 9) indicate that the lithiation process is affected by the presence of $La_{0.8}Sr_{0.2}MnO_3$. The $La_{0.8}Sr_{0.2}MnO_3$ coated NiO cathode samples improve the charge transfer processes associated with the oxygen reduction. In brief, the semicircular arc for two cathode materials shows significant variations during the 200 h of immersion, which can be attributed to the changes in the structure of the reactive surfaces of cathode materials due to the lithiation and slow dissolution of cathode materials. After that, the diameter of the semicircular arc does not increase fundamentally, and the structure seems to reach a stable state. However, more work is required to confirm the long-term electrochemical characterization of the LSM–NiO cathode.

Figure 14 shows the impedance response of LSM–NiO cathode as a function of different gas compositions at 200 h at 650 °C. It can also be seen that the effect of partial pressure of O_2 and CO_2 are antagonistic to each other. The magnitude of the impedance loop decreased on increasing the O_2 partial pressure. This clearly indicates a positive reaction order for oxygen and is similar to the response seen for NiO [38]. In the case of CO_2, the impedance value increased with increase in CO_2 partial pressure implying that the reaction order of CO_2 must be negative.

4. Conclusions

$La_{0.8}Sr_{0.2}MnO_3$ was coated on the state-of-the-art porous NiO cathode using a simple combustion process. $La_{0.8}Sr_{0.2}MnO_3$ coating followed by sintering yielded electrodes with good pore structure. No significant

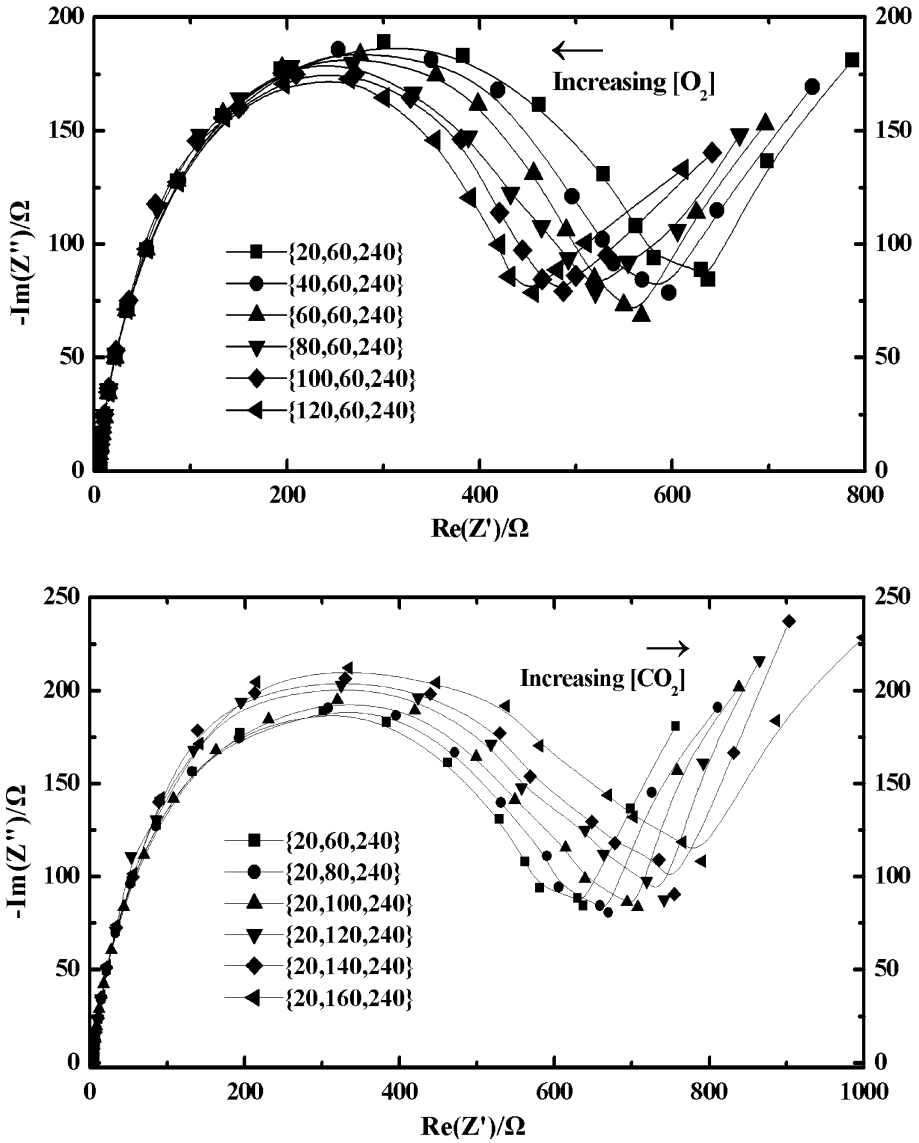

Fig. 14. Nyquist plots of impedance response of LSM–NiO cathode as a function O_2 and CO_2 partial pressure at 650 °C. The numbers in parenthesis "{}" indicates the O_2, CO_2 and N_2 concentrations in cm^3 min^{-1}.

differences in the particle size and the surface morphology of $La_{0.8}Sr_{0.2}MnO_3$-coated NiO cathode were observed before and after immersion in the eutectic molten Li/K carbonates for 200 h.

The short-term stability tests in the eutectic molten Li/K carbonates at 650 °C showed that the coating of $La_{0.8}Sr_{0.2}MnO_3$ on NiO cathode was dramatically effective in reducing NiO dissolution. The impedance response of the NiO and LSM–NiO cathode at different immersion times was characterized by the presence of depressed semicircles in the high frequency range and an extension at low frequencies. Impedance analysis showed that the impedance behavior of the LSM–NiO cathode was similar to that of the conventional NiO cathode. The LSM–NiO showed a better catalytic efficiency superior to the state-of-the-art NiO value. However, extensive pore volume distribution studies need to be done to optimize the pore structure and porosity, which is expected to give optimum electrochemical catalytic efficiency value.

The cathode prepared by a method to coat $La_{0.8}Sr_{0.2}MnO_3$ onto the surface of a NiO cathode was able to reduce the solubility of NiO, and to lengthen the lifetime of MCFC while maintaining even enhancing the advantages of NiO cathode. Therefore, it could be used as an alternative cathode for MCFC. Using this manufacturing method, we expect that economical and large-scale cathodes can be made easily.

References

1. Y. Ito, K. Tsuru, J. Oishi, Y. Miyazaki and K. Teruo, *J. Power Sources* **23** (1988) 357.
2. P. Ganesan, H. Colon, B. Haran, R. White and B.N. Popov, *J. Power Sources* **111** (2002) 109.
3. A. Durairajan, H. Colon-Mercado, B. Haran, R. White and B.N. Popov, *J. Power Sources* **104** (2002) 157.
4. T. Nishina and I. Uchida, *Denki Kagaku Oyobi Kogyo Butsuri* **64** (1996) 513.

5. J. Robert, Y. Hwan, Kim and Selman, *Proc. Electrochem. Soc.* **94** (1994) 781.
6. J.R. Selman, M.S. Alicia and Y. Lzaki, *Prepr. Pap. Am. Chem. Soc., Div. Fuel Chem.* **38** (1993) 1429.
7. W.H.A. Peelen, M.V. Driel, K. Hemmes and J.H.W.D. Wit, *Electrochim. Acta* **43** (1998) 3313.
8. T. Ogawa, H. Oozu, K. Murata and T. Shirogami, *Jpn. Electrochem.* **56** (1988) 791.
9. T. Ogawa, H. Oozu, K. Murata and T. Shirogami, *Jpn. Electrochem.* **58** (1990) 336.
10. K. Tanimoto, Y. Miyazaki, M. Yanagida, S. Tanabe, K. Kojima, N. Ohtori, H. Okuyama and T. Kodama, *J. Power Sources* **39** (1992) 285.
11. J.L. Smith, G.H. Kucera and A.P. Brown, *in* Molten Carbonate Fuel Cell Technology, PV90-16, The Electrochemical Society Softbound Proceedings Series (Pennington NJ, 1990), pp. 226.
12. S.T. Kuk, Y.S. Song and K. Kim, *J. Power Sources* **83** (1999) 50.
13. L. Daza, C.M. Rangel, J. Baranda, M.T. Casais, M.J. Martinez and J.A. Alonso, *J. Power Sources* **86** (2000) 329.
14. T. Fukui, S. Ohara, H. Okawa, T. Hotta, M. Naito and T. Yokoyama, *J. Power Sources* **86** (2000) 340.
15. T. Fukui, H. Okawa, T. Hotta and M. Naito, *J. Am. Ceram. Soc.* **84** (2001) 233.
16. B. Fang and H. Chen, *J. Electroanal. Chem.* **501** (2001) 128.
17. S.T. Kuk, Y.S. Song, S. Suh, J.Y. Kim and K. Kim, *J. Mater. Chem.* **11** (2001) 630.
18. F. Li, H.Y. Chen, C.M. Wang and K.A. Hu, *J. Electroanal. Chem.* **531** (2002) 53.
19. J. Han, S.G. Kim, S.P. Yoon, S.W. Nam, T.H. Lim, I.H. Oh, S.A. Hong and H.C. Lim, *J. Power Sources* **106** (2002) 153.
20. S.G. Kim, S.P. Yoon, J. Han, S.W. Nam, T.H. Lim, S.A. Hong and H.C. Lim, *J. Power Sources* **112** (2002) 109.
21. S. Mitsushima, K. Matsuzawa, N. Kamiya and K. Ota, *Electrochim. Acta* **47** (2002) 3823.
22. P. Ganesan, H. Colon, B. Haran and B.N. Popov, *J. Power Sources* **115** (2003) 12.
23. C. Belhomme, E. Gourba, M. Cassir and C. Tessier, *J. Electroanal. Chem.* **503** (2001) 69.
24. J. Soler, T. Gonzalez, M.J. Escudero, T. Rodrigo and L. Daza, *J. Power Sources* **106** (2002) 189.
25. H.J. Choi, S.K. Ihm, T.H. Lim and S.A. Hong, *J. Power Sources* **61** (1996) 239.
26. F. Li, C.M. Wang and K.A. Hu, *Mater. Res. Bull.* **37** (2002) 1907.
27. B. Huang, F. Li, Q.C. Yu, G. Chen, B.Y. Zhao and K.A. Hu, *J. Power Sources* **128** (2004) 135.
28. S. Jain, K. Adiga and V. Vrneker, *Combust. Flame* **40** (1981) 71.
29. A.J. Appleby and S.B. Nicholson, *J. Electroanal. Chem.* **53** (1974) 105.
30. I. Uchida, T. Nishina, Y. Mugikura and K. Itaya, *J. Electroanal. Chem.* **206** (1986) 229.
31. N. Motohira, T. Sensou, K. Yamauchi, K. Ogawa, X. Liu, N. Kamiya and K. Ota, *J. Mol. Liq.* **83** (1999) 95.
32. S. Iseki, K. Ohashi and S. Nagaura, *Electrochim. Acta* **17** (1972) 2249.
33. J. Wang, C.Y. Shi, S.Z. Song and C.N. Cao J. Chinese Soc. Corros. Protection 13 (1989) 12.
34. J.N. Sarmousakis and M.J. Prager, *J. Electrochem. Soc.* **104** (1957) 454.
35. R. DE Levie, *Electrochim. Acta* **10** (1965) 113.
36. G.M. Schmid, *Electrochim. Acta* **15** (1970) 65.
37. F. Mansfeld and M.W. Kendig *in* G.S. Havenes, R. Baboian (Eds.) Laboratory Corrosion Tests and Standards, ASTM STP 866 (American Society and Materials, Philadelphia PA, 1985) pp. 122.
38. C.Y. Yuh and J.R. Selman, *J. Electrochem. Soc.* **138** (1991) 3649.